

Individual Addressing of Trapped Ions and Coupling of Motional and Spin States Using rf Radiation

M. Johanning,¹ A. Braun,¹ N. Timoney,¹ V. Elman,¹ W. Neuhauser,² and Chr. Wunderlich¹

¹*Fachbereich Physik, Universität Siegen, 57068 Siegen, Germany*

²*Institut für Laser-Physik, Universität Hamburg, Luruper Chaussee 149, 22761 Hamburg, Germany*

(Received 30 May 2008; published 20 February 2009)

Individual electrodynamically trapped and laser cooled ions are addressed in frequency space using radio-frequency radiation in the presence of a static magnetic field gradient. In addition, an interaction between motional and spin states induced by an rf field is demonstrated employing rf optical double resonance spectroscopy. These are two essential experimental steps towards realizing a novel concept for implementing quantum simulations and quantum computing with trapped ions.

DOI: 10.1103/PhysRevLett.102.073004

PACS numbers: 37.10.Vz, 03.67.-a, 32.60.+i, 37.10.Ty

Quantum simulations addressing a specific scientific problem and universal quantum computation are expected to yield new insight into as of yet unsolved physical problems that withstand efficient treatment on a classical computer (e.g., [1]). Already a small number of qubits (i.e., a few tens) used for quantum *simulations* could solve problems even beyond the realm of quantum-information science. Creating and investigating entanglement in large physical systems is a related important experimental challenge with implications for our understanding of the transition between the elusive quantum regime and the classical world [2].

Laser cooled atomic ions confined in an electrodynamic cage have successfully been used for quantum-information processing [3], and advantages and difficulties associated with this system have been and still are subject to detailed investigations. The electromagnetic radiation used to coherently drive ionic resonances that serve as qubits needs to be stable against variations in frequency, phase, and amplitude over the course of a quantum computation or simulation. Experimentally this is particularly challenging when laser light is used for realizing quantum gates. When employing laser light, additional issues need to be dealt with to allow for accurate qubit manipulation, such as the intensity profile of the laser beam, its pointing stability, and diffraction effects. Furthermore, the motional state of the ion chain strongly affects the gate fidelity which requires ground state cooling and low heating rates during the gate operation [4]. Also, spontaneous scattering of laser light off excited electronic states may pose a limit for the coherence time of a quantum many-body state. The probability for scattering can be reduced by increasing the detuning from excited states (when two laser light fields are used that drive a Raman transition between hyperfine or Zeeman states), which, however, leads to an increasing demand for laser power [5].

For generating Raman laser beams with a desired frequency difference, first a radio-frequency (rf) or microwave signal at this difference frequency has to be generated that is then “imprinted” on the laser light and sent to the

ions. Using rf or microwave radiation directly for coherent driving of qubit transitions is impeded in usual ion trap schemes, since (i) individual addressing of qubits by focusing radiation on just one ion is difficult due to the long wavelength of rf radiation and (ii) the required coupling between qubit states and motional states (that serve as a quantum bus [6]) as measured by the Lamb-Dicke parameter is negligibly small. Here, we demonstrate individual addressing of trapped ions in frequency space instead of position space using rf radiation, thus avoiding the technical and fundamental difficulties mentioned above that are associated with the use of laser light for coherent manipulation of trapped ions.

This is achieved by applying a spatially varying magnetic field such that the relevant Zeeman states of each ion exhibit a site-specific resonance frequency. Also, this magnetic gradient field mediates coupling between Zeeman states and motional states [7]. Such a coupling is required, for instance, for conditional quantum dynamics (quantum gates) with two or more ions. It may also be used for any experiment where coupled dynamics of motional and spin states is desired, for instance, sideband cooling of trapped atoms or ions [8].

At the same time, these are two fundamental experimental steps undertaken on the way towards realizing a novel physical system for quantum-information science, the ion spin molecule. The term ion spin “molecule” is used here to describe a pseudomolecule [9] exposed to a magnetic field gradient that induces pairwise coupling J_{ij} between the internal qubit states (spins) of ion i and j ($i, j = 1, 2, 3, \dots, N$ with N the number of ions) [10,11]. An ion spin molecule is useful for quantum simulations, since spin chains with globally and locally adjustable coupling parameters can be realized and are well suited, for instance, for simulating magnetism of quantum systems [12]. Also, ion spin molecules may be used to implement a classical neural network or error-resistant quantum computing based on a quantum neural network [13].

The experiments presented here were performed with laser cooled $^{172}\text{Yb}^+$ ions in a linear Paul trap. A detailed

description of the trap and the experimental setup is given in [14]. The electric dipole transition between the $S_{1/2}$ ground state and the $P_{1/2}$ excited state near 369 nm is used for Doppler cooling and state-selective detection by detecting resonance fluorescence with a photomultiplier or an intensified CCD camera (“cooling fluorescence”). Individual addressing of ions and the coupling between motional and internal ionic states is demonstrated using rf optical double resonance spectroscopy on the metastable $D_{3/2}$ state (lifetime of 52.2 ms [15]) populated through spontaneous decay from the $P_{1/2}$ level. The degeneracy of its Zeeman manifold is lifted by a magnetic field $B = B_0 + z\partial_z B$ composed of an offset field B_0 and an additional field with constant gradient $\partial_z B$ (\vec{z} is the axis of rotational symmetry of the trapping potential and thus of the linear ion string). The magnitude of B determines the resonance frequency of magnetic dipole transitions between Zeeman states. The (linear) Zeeman shift ΔE_J by a magnetic field B is given by $\Delta E_J = g_J m_J \mu_B B$ with Landé g -factor g_J , magnetic quantum number m_J and the Bohr magneton μ_B . Magnetic dipole transitions between levels with $\Delta m_J = \pm 1$ with resonance frequency $f = g_J \mu_B B/h$ are driven using an rf field that is generated by a dipole coil. The magnitude of B_0 was chosen for most experiments to be about 0.67 mT, resulting in a resonance frequency $f \approx 7.5$ MHz.

This four level system can be initialized by optical pumping: a laser light field near 935 nm [16] (labeled “repumper” in what follows) with its linear polarization aligned parallel to \vec{B} allows π transitions ($\Delta m = 0$) only. Since repumping occurs through the state $[3/2]_{1/2}$ with $m = \pm 1/2$, population accumulates in the “dark” $m = \pm 3/2$ states, and in turn the resonance fluorescence near 369 nm stops. Upon coupling the Zeeman sublevels with a resonant rf field the resonance fluorescence reappears. Modeling the ionic dynamics in the stationary state using rate equations shows the intensity of scattered light near 369 nm to be proportional to the population in the $D_{3/2}$ Zeeman states with $m = \pm 1/2$. The stationary state is obtained when the cooling laser, the repumper, and the rf field are applied simultaneously and the magnetic field is aligned parallel to the polarization of the repumper to allow for optical pumping. Then rf optical double resonance spectra are observed. When the rf is scanned across this resonance frequency, Lorentzian line shapes are observed whose linewidth is determined by the intensity of both the rf radiation and the laser light near 935 nm (repumper). We observed linewidths between 15 kHz and 310 kHz for rf powers between 25 mW and 8 W and repumping powers between 0.3 and 3.8 μ W focused to a spot size of approximately 100 μ m in diameter. For a vanishing gradient $\partial_z B$, all ions have the same resonance frequency f determined by the offset field B_0 .

Addressing of individual ions is achieved without focusing the radiation down to less than the spatial separation of adjacent ions by now applying a spatially varying magnetic field $B = B_0 + z\partial_z B$ such that the Zeeman shift is different

for each ion. The frequency separation of the resonances of two neighboring ions is given by

$$\Delta f = g_J \mu_B \delta z \partial_z B/h \quad (1)$$

with ion separation δz . The inhomogeneous field along the trap axis is created by cylindrical Nd permanent magnets with a diameter of 30 mm in quadrupole configuration separated by approximately 12 cm. The magnetic flux density at the surface of the permanent magnets exceeds 1 T.

When scanning the rf frequency, one ion after the other comes into resonance and consequently scatters light. The resonance fluorescence spectra in Fig. 1 show individual addressing of strings of up to three ions with well resolved peaks each corresponding to a resonance of an individual trapped ion. The axial trap frequency was measured by parametric heating to be 36.3(5) kHz, yielding ion separations of 31.7(3) μ m for two ions and 25.0(2) μ m for three ions, respectively. (The radial trap frequency was ≈ 600 kHz.) The experimentally determined frequency separation of the ionic resonances (Fig. 1) together with Eq. (1) yield the magnitude of the field gradient $\partial_z B = 0.27(1)$ T/m. The maximum gradient observed was 0.51(2) T/m. Thus frequency separations of up to 130 kHz could be achieved, and with a line width of 15 kHz, unwanted excitation of vicinal ions is reduced to below 0.4%. Figure 2 is composed of spatially resolved images showing a string of four ions taken with an intensified CCD camera while setting the rf frequency to specific values that correspond to individual ionic resonances. It demonstrates that the peaks of the resonance fluorescence observed in Fig. 1 indeed originate from different ions. Moreover, it shows that single ions are selectively re-

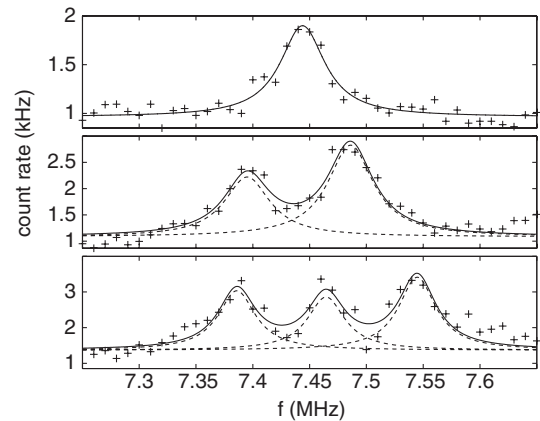


FIG. 1. Individual addressing in frequency space of one (top), two (middle), and three (bottom) trapped ions, respectively. The frequency separation between neighboring ions is extracted by fitting a sum of Lorentzian line profiles and is 91(3) kHz for two ions and 79(4) kHz (middle, left) and 80(4) kHz (middle, right) for three ions. The average ratio of these frequency separations is 1.15(7), which is in good agreement with the analytical prediction of $\sqrt[3]{8/5} \approx 1.17$ for a constant gradient. Together with the extracted FWHM of 49(5) kHz, the spurious excitation of adjacent ions is 6.7(8)% in the case of two ions.

pumped by setting the rf frequency to a particular individual ionic resonance. Here, the spatial separation of the outer ions is $61.3 \mu\text{m}$ (trap frequency of $2\pi \times 46 \text{ kHz}$). Using Eq. (1) this yields a gradient of 0.24 T/m for this experiment.

When a trapped ion interacts with electromagnetic radiation, this may affect not only the atom's internal state but also its motional state evidenced by motional sidebands in an ionic excitation spectrum [17]. The coupling between internal and motional dynamics of the ion is exploited in ion traps to realize conditional quantum dynamics, for instance, a controlled-NOT (CNOT) gate [3,6,18]. The Lamb-Dicke parameter, η , determines its strength: $\eta = \sqrt{\hbar^2 k^2 / 2m\hbar\nu_1}$. Here, the wave number $k = 2\pi/\lambda$, where λ is the wavelength of the radiation exciting the ion, m the ion's mass, and ν_1 the secular vibrational frequency. η is negligibly small when using rf or microwave radiation in contrast to optical fields. For the interaction in an inhomogeneous magnetic field, however, the Zeeman energy and thus the ion's equilibrium position may become state dependent. The coupling of the internal and motional state is now described by an *effective* Lamb-Dicke parameter η_{eff} , which, for a single ion, is given by the ratio between the frequency change of the resonance over the spatial extension $\Delta z = \sqrt{\hbar/2m\nu_1}$ of the ion's wave function and the trap frequency [7]: $|\eta_{\text{eff}}| = \sqrt{\eta^2 + \kappa^2} \approx |\kappa| = \left| \frac{\Delta z \partial_z f_{\text{rf}}}{\nu_1} \right|$. Here, the experimentally determined parameters for the magnetic field gradient and trap frequency yield $\eta_{\text{eff}} = 1.1 \times 10^{-3}$.

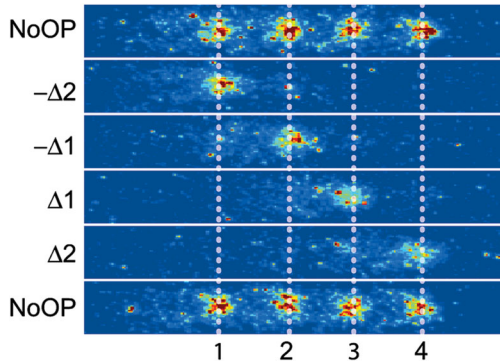


FIG. 2 (color). Individually addressing a particular ^{172}Yb ion that is part of a linear Coulomb crystal composed of four ^{172}Yb ions. Six images of the same ion string are shown. These were taken successively from top to bottom. The uppermost and lowermost image, labeled NoOP, are recorded with no optical pumping; that is, all ions scatter light. For the intermediate pictures, the magnetic field direction is rotated to coincide with the polarization of the repumper, allowing optical pumping. In addition, the rf frequency was set to the expected resonance of one particular ion. The detuning $\Delta 1$ or $\Delta 2$ of the rf frequency necessary to address a desired ion is indicated on the left-hand side of the graph and is given relative to the Zeeman resonance of a single ion. Here, $\Delta 1 = 26.3 \text{ kHz}$ and $\Delta 2 = 83.2 \text{ kHz}$. Here the amount of spurious excitation of adjacent ions is comparable to the crosstalk visible in Fig. 1.

Neglecting saturation, the amplitudes of the lower and upper motional sidebands have a relative height compared to the carrier given by

$$\frac{a_l}{a_0} = \langle n \rangle \eta_{\text{eff}}^2 \quad \text{and} \quad \frac{a_u}{a_0} = (\langle n \rangle + 1) \eta_{\text{eff}}^2 \quad (2)$$

with $\langle n \rangle$ being the mean phonon number [17], and for large $\langle n \rangle$ we have $a_l \approx a_u \equiv a_s$.

The spectra shown in Fig. 3 differ only in the magnetic field B applied to the ion: B is homogeneous for the left spectrum (i.e., $\partial_z B_1 = 0$ and thus $\eta_{\text{eff}} = 0$), while a field gradient is applied for the right spectrum. The measurement procedure is in principle as detailed above, with alternating rf optical double resonance (total duration of 150 ms) and cooling cycles (duration of 100 ms). However, in order to resolve the motional sideband with sufficient signal-to-noise ratio, additional measures have been taken: CCD images are taken simultaneously with the rf scans during the cooling cycles, and preceding each measurement, a fast rf scan through the resonance of the single ion is executed. This ensures single ion operation and excludes drifts of the resonance due to slow field fluctuations. During an optical double resonance measurement the frequency is set alternatingly to seven discrete detunings Δ : $\Delta = 0 \text{ kHz}$ to measure the maximal resonance fluorescence rate for normalization, $\Delta = \pm 15 \text{ kHz}$ to ensure an unchanged center frequency, $\Delta = \pm 250 \text{ kHz}$ to measure the background, and a variable detuning $\pm \Delta$ that is different for each of these measurement cycles. A measurement cycle for a given value of Δ is repeated typically 40 times, and finally data points with equal magnitude of Δ are averaged and the background is subtracted.

The data sets with and without field gradient and the corresponding nonlinear regressions can be compared quantitatively in terms of the goodness of fit Q as defined in [19]. While the left data set (no gradient) is well

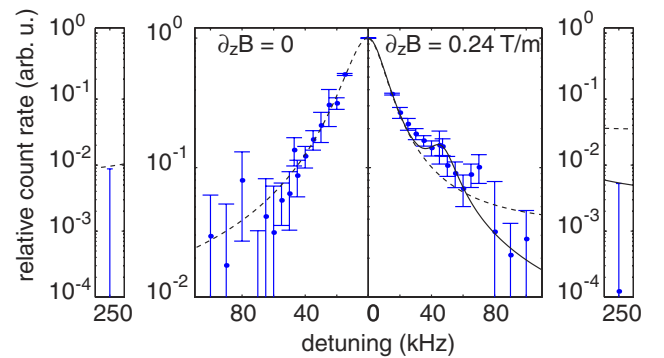


FIG. 3 (color online). A spectrum recorded with a single ion exposed to a magnetic field gradient (right-hand side) compared to one recorded with a single ion without a field gradient (left-hand side). The solid line represents a fit using two Lorentzian lines (right-hand side), and the dashed lines represent fits using a single Lorentzian (left-hand side and right-hand side). The motional sideband accompanying the spin resonance signifies coupling between spin degrees of freedom and the motion of the trapped Yb^+ ion.

described by a single Lorentzian, quantified by a goodness of fit of $Q = 0.95$, the line profile is substantially altered when a gradient is applied (right-hand side), showing a sideband structure at the axial trap frequency that is determined independently by parametric heating to 46.0(5) kHz. A fit with a single Lorentzian (dashed line in Fig. 3) matches the data set poorly and gives $Q = 9.6 \times 10^{-9}$, 5 orders of magnitude below recommended values, to reject the model used for the fit [19]. Modeling the data by a sum of two Lorentzians (carrier and sideband) yields good agreement quantified by $Q = 0.92$.

For the relative height of the motional sideband we obtain $a_s/a_0 = 0.084(8)$. From this ratio, $\langle n \rangle = 6.9(6) \times 10^4$ —corresponding to a temperature $T = 306(30)$ mK—is deduced using Eq. (2) with η_{eff} independently extracted from the addressing measurements presented above. This temperature is substantially higher than the Doppler temperature T_D for Yb ions ($T_D \approx 470 \mu\text{K}$). It is due to the delay time of 50 ms between cooling the ion and performing the measurements, and the low cooling efficiency during the measurement itself (for 100 ms). Other researchers have observed similar temperatures with $^{172}\text{Yb}^+$ [16,20]. For this demonstration of the coupling between spin and motional states of trapped ions in a magnetic field gradient [21], a higher temperature is in fact advantageous, since it increases the relative height of the motional sideband. However, for future experiments the heating rate and temperature of the ions need to be reduced, though ground state cooling is not required to obtain high gate fidelities when using ion spin molecules.

To make full use of the advantages that magnetic gradient induced coupling and the concept of an ion spin molecule offer, substantially higher magnetic field gradients have to be applied in the future. This will allow for better resolution of individual ionic resonances and—since then the Rabi frequency may be increased, too—for fast gate operations. When increasing the number of ions in a linear trap, their spatial separation decreases, again making necessary a larger field gradient to separate neighboring resonances. An expression relating the necessary field gradient for a given small value of crosstalk to the number of ions and the axial trap frequency is given in [7]. The use of microstructured ion traps [22] that are currently under development will give gradients up to 100 T/m, thus making about 40 Yb ions distinguishable in frequency space at a trap frequency of $2\pi \times 260$ kHz. Also, the effective Lamb-Dicke parameter scales linearly with the field gradient, and the spin-spin coupling constants J_{ij} with the square of the gradient. Thus, coupling constants useful for quantum-information processing and quantum simulations will be attained with such traps.

Long-lived ground state hyperfine states of $^{171}\text{Yb}^+$ are well suited as a qubit for further experiments [11,14,23]. Higher Rabi frequencies (i.e., strong coupling between rf or microwave radiation and qubit) will be achieved in the future by using microstructured elements for generating rf or microwave radiation integrated into an ion trap.

We thank Chr. Schneider for support in operating the experiment. Financial support by Deutsche Forschungsgemeinschaft and the European Union (IP QAP) is acknowledged.

-
- [1] R.P. Feynman, *Int. J. Theor. Phys.* **21**, 467 (1982); S. Lloyd, *Science* **273**, 1073 (1996); A. Aspuru-Guzik *et al.*, *Science* **309**, 1704 (2005); D. Porras and J.I. Cirac, *Phys. Rev. Lett.* **93**, 263602 (2004).
 - [2] W. Dür and H.-J. Briegel, *Phys. Rev. Lett.* **92**, 180403 (2004); A. R. R. Carvalho, F. Mintert, and A. Buchleitner, *Phys. Rev. Lett.* **93**, 230501 (2004).
 - [3] F. Schmidt-Kaler *et al.*, *Nature (London)* **422**, 408 (2003); D. Leibfried *et al.*, *Nature (London)* **422**, 412 (2003); K.-A. Brickman *et al.*, *Phys. Rev. A* **72**, 050306(R) (2005); J.P. Home *et al.*, *New J. Phys.* **8**, 188 (2006).
 - [4] D. J. Wineland *et al.*, *J. Res. Natl. Inst. Stand. Technol.* **103**, 259 (1998).
 - [5] A.M. Steane, *Quantum Inf. Comput.* **7**, 171 (2007).
 - [6] J.I. Cirac and P. Zoller, *Phys. Rev. Lett.* **74**, 4091 (1995); A. Sørensen and K. Mølmer, *Phys. Rev. A* **62**, 022311 (2000); D. Jonathan, M. B. Plenio, and P.L. Knight, *Phys. Rev. A* **62**, 042307 (2000).
 - [7] F. Mintert and C. Wunderlich, *Phys. Rev. Lett.* **87**, 257904 (2001); **91**, 029902(E) (2003).
 - [8] C. Wunderlich, G. Morigi, and D. Reiss, *Phys. Rev. A* **72**, 023421 (2005).
 - [9] D.J. Wineland *et al.*, *Phys. Rev. Lett.* **59**, 2935 (1987).
 - [10] C. Wunderlich, in *Laser Physics at the Limit*, edited by H. Figger, D. Meschede, and C. Zimmermann (Springer, Berlin, 2002); D. McHugh and J. Twamley, *Phys. Rev. A* **71**, 012315 (2005).
 - [11] C. Wunderlich and C. Balzer, *Adv. At. Mol. Phys.* **49**, 293 (2003).
 - [12] A. Friedenauer *et al.*, arXiv:0802.4072.
 - [13] M. Pons *et al.*, *Phys. Rev. Lett.* **98**, 023003 (2007); S. Braungardt, A. Sen(De), U. Sen, and M. Lewenstein, *Phys. Rev. A* **76**, 042307 (2007).
 - [14] C. Balzer *et al.*, *Phys. Rev. A* **73**, 041407(R) (2006).
 - [15] C. Gerz *et al.*, *Z. Phys. D* **8**, 235 (1988).
 - [16] A. S. Bell *et al.*, *Phys. Rev. A* **44**, R20 (1991).
 - [17] D.J. Wineland and W.M. Itano, *Phys. Rev. A* **20**, 1521 (1979); J.C. Bergquist *et al.*, *Phys. Rev. A* **36**, 428 (1987).
 - [18] C. Monroe *et al.*, *Phys. Rev. Lett.* **75**, 4714 (1995).
 - [19] W.H. Press *et al.*, *Numerical Recipes: The Art of Scientific Computing* (Cambridge University Press, Cambridge, England, 2007), Chap. 15.1.
 - [20] D. Kielpinski, M. Cetina, J.A. Cox, and F.X. Kärtner, *Opt. Lett.* **31**, 757 (2006).
 - [21] For experimental work with trapped electrons, see, for instance, R.S. Van Dyck, Jr., *et al.*, *Phys. Rev. Lett.* **38**, 310 (1977). Recent theoretical work on trapped electrons includes G. Ciaramicoli *et al.*, *Phys. Rev. A* **72**, 042323 (2005).
 - [22] S. Seidelin *et al.*, *Phys. Rev. Lett.* **96**, 253003 (2006); D. Stick *et al.*, *Nature Phys.* **2**, 36 (2006); C. Ospelkaus *et al.*, arXiv:0805.2165.
 - [23] S. Olmschenk *et al.*, *Phys. Rev. A* **76**, 052314 (2007).